Electronic Supplementary Information:

Evaluating the techno-economic potential of defossilized air-to-syngas pathways

Hussain M. Almajed[a,b], Omar J. Guerra[c], Wilson A. Smith[a,b,c,d], Bri-Mathias Hodge*[b,c,e,f] and Ana Somoza-Tornos*[b,d]

[a.] Department of Chemical and Biological Engineering, University of Colorado Boulder, Boulder, CO 80309, USA.

[b.] Renewable and Sustainable Energy Institute, University of Colorado Boulder, Boulder, CO 80309, USA.

[c.] National Renewable Energy Laboratory, Golden, CO, 80401, USA.

[d.] Delft University of Technology, Department of Chemical Engineering, Van der Maasweg 9, 2629 HZ Delft, The Netherlands.

[e.] Department of Electrical, Computer, and Energy Engineering, University of Colorado Boulder, Boulder, CO 80309, USA.

[f.] Department of Applied Mathematics, University of Colorado Boulder, Boulder, CO 80309, USA.
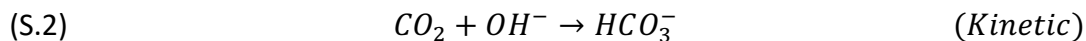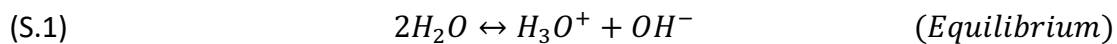
Table of Contents

S.1. Process modeling

S.1.1. Direct air CO_2 capture (DACC)

We developed our DACC plant model in Aspen Plus using modeling and flow rate information from several of Carbon Engineering's publications[1–3] as well as from other researchers[4,5] who attempted to model the hydroxide-based DACC plant. Our model leverages the Electrolyte Non-Random Two-Liquid (ELECNRTL) thermodynamic model to account for like-ion repulsion and electroneutrality.[6] Following Keith et al.'s method,[1] we added the ASPENPCD, AQUEOUS, INORGANIC, PURE26, and SOLIDS databanks to the ELECNRTL default databanks.

To begin, we modeled the air contactor using a built-in rate-based RADFRAC model, operating at 25℃ and 1 atm. The modeling specifications, flow rates, and fractions are shown in Tables S.1, S.2, and S.3, respectively. We chose a packing height and diameter of 8.3 m and 4.0 m, respectively, similar to the optimized air travel distance (7 m) and diameter (5 m) of Carbon Engineering's air contactor design.[1] The difference in height and diameter most likely comes from the different flow configurations; our RADFRAC unit assumes a counter-flow configuration whereas the CE air contactor operates in a cross-flow mode. We additionally accounted for pressure drop through the contactor by adding a pressure drop of 127.515 Pa, corresponding to the calculated pressure drop using data from Carbon Engineering.[1,2] Moreover, we attached two kinetic and two equilibrium reactions (Eqs. S.1–S.4) to the air contactor model along with their pre-exponential factors and activation energies (see Table S.4 for kinetic data and Table S.5 for equilibrium data) to simulate the CO_2 capture process using hydroxides. We chose a standard MELLAPAK Sulzer 250X column packing and changed its specific surface area (SSA) to be equivalent to that of Brentwood XF12560 packing (i.e., 210 m^2/m^3)(1). The choice of packing was motivated by Heidel et al.'s[3] study that demonstrates the similar capture behavior of the two mentioned packings. Our modular air contactor model was designed to capture 633 t-CO_2/yr, consistent with the estimate given by Keith and colleagues (i.e. 160 units can capture about 100 kt-CO_2/yr).[1] Consequently, we were able to use it for any capture amount needed.

$$(S.1) \qquad 2H_2O \leftrightarrow H_3O^+ + OH^- \qquad (Equilibrium)$$

$$(S.2) \qquad CO_2 + OH^- \rightarrow HCO_3^- \qquad (Kinetic)$$

$$(S.3) \qquad HCO_3^- \rightarrow CO_2 + OH^- \qquad (Kinetic)$$

(S.4) $$HCO_3^- + H_2O \leftrightarrow CO_3^{2-} + H_3O^+ \qquad (Equilibrium)$$

Table S.1. Modeling specifications.

RADFRAC Specifications	
Number of Stages	16
Calculation Type	Rate-Based
Condenser?	No
Reboiler?	No
Valid Phases	Vapor-Liquid
Convergence Type	Standard
Pressure Drop	127.515 Pa
Liquid and Gas Feed Temperature	21 ˚C
Operating Liquid and Gas Feed Pressure	1 atm
Liquid Feed Stage	16, On-Stage
Air Feed Stage	1, On-Stage
Stage 1 Pressure	1 atm
Column Specifications	
Starting Stage	1
Ending Stage	16
Mode	Rating
Internal Type	Packed
Packing Type	MELLAPAK

Vendor	Sulzer
Material	Standard
Dimensions	250X
Section Packed Height	7 m
Diameter	5.642 m
Design Specification	
Mass Recovery Ratio	0.255
Vary Parameter	
Air Feed Rate	21,000 – 25,000 kmol/hr
Reaction Specifications	
Reactions Included	Equations (S.1) – (S.4)
Starting Stage	1
Ending Stage	16
Residence Time	0.001 sec

Table S.2. Mass and mole flow rates.

Stream	Mass Flow Rate (kg/hr)	Molar Flow Rate (kmol/hr)
Air Inlet	674,000	23,496.2
Sorbent Inlet	12,400	650.745
Liquid Product	674,953	23,559
Depleted Air	11,447	581.109

Table S.3. Mass and mole fractions.

Component	Air Inlet	Sorbent Inlet	Liquid Product	Depleted Air
CO_2	0.0006	1.165E-14	0.000152	2.487E-08

H_2O	0.0098	0.8872	0.0116	0.8602
K^+	0	0.0712	0	0.0771
CO_3^{2-}	0	0.0246	0	0.0557
O_2	0.23	0	0.2297	6.134E-06
N_2	0.7596	0	0.7585	1.018E-05
HCO_3^-	0	2.653E-06	0	0.00694
H_3O^+	0	1.588E-16	0	5.293E-14
OH^-	0	0.0170	0	2.361E-05
KOH	0	0	0	0
K_2CO_3	0	0	0	0
$KHCO_3$	0	0	0	0

Table S.4. Kinetic data.

Reaction	k	n	$E_{activation}$ (kJ/mol)	Notes	Reference
(S.2)	$4.20 \bullet 10^{13}$	0	55.385	T-Range: $0 - 40$ ˚C	Pinsent et al.(7)
(S.3)	$2.38 \bullet 10^{17}$	0	123.22		

Table S.5. Equilibrium data.

Reaction	A	B	C	D	Notes	Reference
(S.1)	140.932	-13445.9	-22.4773	0	T-Range: $0 - 225$ ˚C	Edwards et al.(8)
(S.4)	220.067	-12431.7	-35.4819	0		

We also modeled the pellet reactor, slaker, and calciner in Aspen Plus to create an integrated DACC process. We used built-in stoichiometric reactors (i.e., RStoic) that assume the absence of kinetic limitations and require reaction information along with a fractional conversion percentage for each. We defined Eqs. 2 and 3, in the main text, to be the only active reactions inside the pellet reactor and slaker, respectively, with fractional conversions of 90% of $Ca(OH)_2$ and 85% of
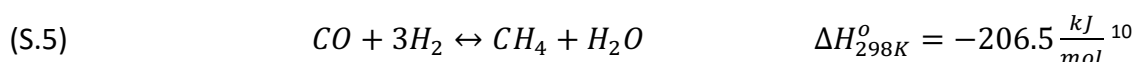
CaO, as provided by Keith and colleagues.[1] Finally, we considered the calcination of 98% of $CaCO_3$ and the combustion of 100% of CH_4 in the calciner unit.
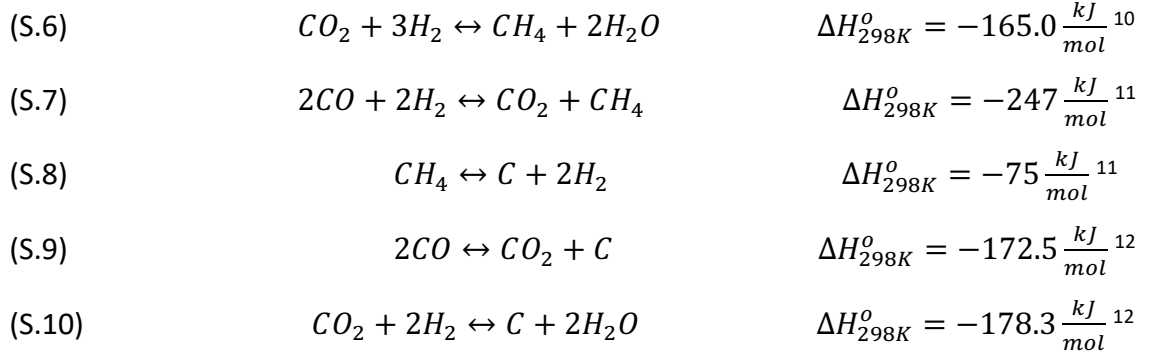
In addition to the major DACC equipment, the present model considers quicklime mixing, power generation using a Heat Recovery Steam Generation (HRSG) setup, and some downstream processing. The quicklime mixing is modeled using a stoichiometric reactor (RStoic) to allow for the remaining CaO to convert fully into $Ca(OH)_2$. Power generation was modeled using a Gibbs reactor (RGibbs) to simulate the combustion of methane before supplying the heat into an HRSG unit, which was modeled using a heat exchanger (MHeatX). Finally, downstream processing is dependent on the conditions required for storage or utilization. To reproduce Keith et al.'s results,[1] we consider downstream processing to include dehydration as well as multi-stage compression to 150 bar with in-between stage coolers. However, for integration with RWGS or CO_2ER, we consider downstream processing to include a dehydration step followed by a cooling step. Further information about the model can be found in the SI.

S.1.2. Reverse water gas shift (RWGS)

The referenced RWGS model was built in Aspen Plus by Rezaei and Dzuryk.[9] They were able to feed in a mixture of CO_2 and H_2 at an H_2:CO_2 molar ratio of 2.85 to a fired heater (RWGS reactor) at 945 ℃ and 4.1 bar, achieving a CO_2 molar conversion of about 77%. The gaseous outlet is then fed to an amine-based CO_2 absorption process, in which CO_2 is captured using a monoethanolamine (MEA) liquid solvent. The products are finally compressed, dehydrated, and heated to have a final temperature and pressure of 200 ℃ and 30 bar, respectively. The production rate was calculated to be 22,575.6 kmol-syngas/hr (equivalent to 2.12 Mt-syngas/yr for 100% plant utilization) and the molar ratio of syngas was set to 2. The reported equipment duties, annual CAPEX, and steam utility costs were referenced in this study to estimate the 2021-extrapolated annual CAPEX, OPEX, and total syngas cost of the DACC-PEMWE-RWGS pathway. It is worth noting that no new modeling results were obtained for the RWGS because it was used as developed by the authors.

Equations S.5 – S.10 show the Sabatier and carbon formation side reactions:

$$(S.5) \qquad CO + 3H_2 \leftrightarrow CH_4 + H_2O \qquad \Delta H^o_{298K} = -206.5 \frac{kJ}{mol} \,[10]$$

(S.6)	$CO_2 + 3H_2 \leftrightarrow CH_4 + 2H_2O$	$\Delta H_{298K}^o = -165.0\,\frac{kJ}{mol}$ [10]
(S.7)	$2CO + 2H_2 \leftrightarrow CO_2 + CH_4$	$\Delta H_{298K}^o = -247\,\frac{kJ}{mol}$ [11]
(S.8)	$CH_4 \leftrightarrow C + 2H_2$	$\Delta H_{298K}^o = -75\,\frac{kJ}{mol}$ [11]
(S.9)	$2CO \leftrightarrow CO_2 + C$	$\Delta H_{298K}^o = -172.5\,\frac{kJ}{mol}$ [12]
(S.10)	$CO_2 + 2H_2 \leftrightarrow C + 2H_2O$	$\Delta H_{298K}^o = -178.3\,\frac{kJ}{mol}$ [12]

S.1.3. Electrolysis model

Our electrolysis model rigorously performs mass and energy balances of a referenced system to estimate the production rate of our product and the total current needed for electrolysis (Eq. S.11). The electrolyzer area is taken from a reference study and scaled up to produce the needed production rate. This information is then used to estimate the current density (Eq. S.12), relating the total production rate to the current density of our system. Following that, we implement the famous Butler-Volmer equation (Eq. S.13) to correlate the current density to the cell voltage, allowing for more accurate estimates of the total product cost in the sensitivity analysis. However, before using this equation, we need empirical values of the exchange current density ($j_{ex,0}$), the charge transfer coefficient (α), and the activation overpotential (η_{ac}). The first two can be taken from an experimental reference study. The activation overpotential can be estimated from the total cell voltage (V_{cell}), the thermoneutral cell voltage (V_{tn}), and the ohmic overpotential of membrane ($\eta_{ohmic,memb}$), electrolyte ($\eta_{ohmic,electrolyte}$), and bubbles ($\eta_{ohmic,bubble}$). Equations S.14 and S.15 can be used to calculate the thermoneutral cell voltage and estimate the ohmic overpotentials, respectively. F is Faraday's constant, which is equal to 96,485 $A \bullet \frac{mol}{s}$, X_i is the thickness of element i in meters, and κ_i is the electrical conductivity of element i in S/m. i refers to membrane or electrolyte in our case. Equation S.16 can be used to estimate η_{ac}, assuming some value of $\eta_{ohmic,bubble}$. For further information of how we estimate the bubble overpotential, please refer to the next paragraph. From here, we are able to estimate the electrolyzer power consumption (Eq. S.17) and the total electricity consumption of the pressure swing adsorption (PSA) separation (Eq. S.18). $E_{PSA,ref}$ is the reference electricity consumption of

PSA in kWh/m³, $\dot{V}_{cathode}$ is the volumetric flow rate of the gaseous cathodic products in m³/yr, and C_{el} is the electricity price in \$/kWh. In addition to all of these features, our model is able to consider CO_2 losses due to (bi)carbonates that can cross over to the anode side as carbonates. Those are ideally measured experimentally and inputted into the model as loss percentages.

(S.11) $\quad I_{tot} = \left(\dfrac{\dot{m}_{CO}}{MW_{CO}} \bullet z_{e^-,CO} + \dfrac{\dot{m}_{H_2}}{MW_{H_2}} \bullet z_{e^-,H_2} \right) \bullet \dfrac{F}{3600}$

(S.12) $\quad j_{tot} = \dfrac{I_{tot}}{A_{electrode}}$

(S.13) $\quad j_{tot} = j_{ex,0} \left[\exp\left(\dfrac{\alpha \bullet z \bullet F \bullet \eta_{ac}}{RT} \right) - \exp\left(\dfrac{-(1-\alpha) \bullet z \bullet F \bullet \eta_{ac}}{RT} \right) \right]$

(S.14) $\quad V_{tn} = \dfrac{\Delta H_{rxn}}{nF}$

(S.15) $\quad \eta_{ohmic,i} = X_i \dfrac{j_{tot}}{\kappa_i}$

(S.16) $\quad \eta_{ac} = V_{cell} - V_{tn} - \eta_{ohmic,i} - \eta_{ohmic,bubble}$

(S.17) $\quad P = I_{tot} \bullet V_{cell}$

(S.18) $\quad E_{PSA} = E_{PSA,ref} \bullet C_{el} \bullet \dot{V}_{cathode}$

As mentioned above, after estimating the ohmic overpotential of the membrane and electrolyte, we use them in Eq. S.16 to estimate the activation overpotential. However, the total current density, j_{tot}, would result in a different value than the expected one, which is 612 mA/cm² in our case. Thus, we use $\eta_{ohmic,bubble}$ as a tuning knob to allow for j_{tot} to be equal to our expected current density, 612 mA/cm². Thus, we find the ohmic overpotential of the bubble to be approximately 0.1014 V. To complete the calculations, we use the following values to estimate the total current density using Equations S.13, S.14, S.15, and S.16:

- V_{cell} = 3.3 V [13]
- V_{tn} = 1.47 V
- $X_{electrolyte}$ = 1 mm [13]
- $\kappa_{electrolyte}$ = 7.2 S/m
- $X_{membrane}$ = 25 μm [13]
- $\kappa_{membrane}$ = 7.8 S/m [14]
- j_{tot} = 612 mA/cm² (***only used in Eq. S.15, and calculated using equation S.13***)
- α = 0.201 [15]

- $z = 2$ (mol-e$^-$/mol-CO)

- $R = 8.314$ J/(K•mol-CO)

- $T = 298.15$ K

- $j_{ex,0} = 0.000842$ mA/cm^2 [15]

- $\eta_{ohmic,bubble} = 0.1014$ V

S.1.4. Steam methane reforming (SMR)

The referenced SMR process model assumes pure CH_4 and H_2O inlets of 3,160 kmol-CH_4/hr and 9,480 kmol-H_2O/hr, respectively.[9] The model includes a fired heater as well as an absorber and a regenerator to remove CO_2 from the H_2 product stream. The captured CO_2 can either be recycled to the RWGS reactor (when integrated with RWGS) or emitted to the atmosphere. We consider both scenarios in the main text.

At the modeled scale, the SMR plant is able to produce 19,665 kg-H_2/hr whereas the RWGS reactor requires 45,397 kg-H_2/hr. Thus, we linearly scaled up the SMR model by a factor of 2.3 to reach the needed scale for the purposes of our work. Additionally, it is worth noting that the outlet temperature and pressure of H_2 in the modeled SMR process are not identical to the inlet conditions of H_2 in the RWGS plant. However, this fact does not change the conclusions of our presented work as we include the carbon efficiency, energy consumption and cost, and marginal energy-associated CO_2 emissions in our assessment of DACC-SMR-RWGS and exclude the economic metrics. In other words, adding a turbine and a cooler would only increase the energy consumption and cost of DACC-SMR-RWGS, which would not change the outcome of our work.

S.2. Techno-economic assessment (TEA)

The TEA presented here generally follows the method given by Towler and Sinnot.[16] The total product cost per mass (TPC$_{product}$) is simply the summation of the annual capital and operational costs divided by the mass flow rate of the product in kg/yr, Eq. S.19. The following subsections summarize the capital and operational cost calculations and assumptions.

(S.19) $$TPC_{product} = \frac{CAPEX_{annual} + OPEX_{annual}}{\dot{m}_{product}}$$

S.2.1. Capital costs

The purchased equipment cost (PEC) can be estimated using two methods: the bare-module and the Lang-factor methods. The former references an older cost estimate (PEC_{old}) of the same equipment, a sizing parameter (S_{old}), and a scaling factor (n) and requires a new sizing parameter (S_{new}) to be known, as shown in Eq. S.20. The latter method uses two constants (a and b), a new sizing parameter (S_{new}), and a scaling factor (n), Eq. S.21. Both methods are capable of estimating the PEC of an equipment, but the method of choice will depend on the cost information availability and source. For H_2O and CO_2 electrolyzers, the rigorous estimate of a future centralized PEM water electrolyzer given by the H2A production model ($233/kWh)[17] was used because it is considered the state-of-the-art estimate today.[18,19] Although several researchers[20–22] have attempted to estimate the CO_2 electrolyzer CAPEX per m^2 using different methods, their very wide cost range of $960-12,000/$m^2$ indicates the existence of high uncertainty. We acknowledge that this area needs further studies and thus stick with the future estimate of the state-of-the-art H_2O electrolyzer CAPEX for both H_2O and CO_2 electrolyzers here. As a comparison, however, the capital costs of H_2O electrolyzers and CO_2 electrolyzers are equivalent to $8,877/$m^2$ and $4,713/$m^2$, respectively, which fall within the wide range mentioned above.

$$(S.20) \quad PEC = PEC_{old} \left(\frac{S_{new}}{S_{old}}\right)^n$$

$$(S.21) \quad PEC = a + bS_{new}^n$$

The installed equipment cost (IEC) was calculated by multiplying an appropriate installation factor ($f_{installation}$) by the respective PEC using Eq. S.22. Table S.6 summarizes a full list of installation factors used in this study and for details on which PEC equation is used for which equipment. Further, extrapolation to 2021 costs was performed using the chemical engineering plant cost index (CEPCI), as shown by Eq. S.23, in which IEC_{old}, IEC_{2021}, $CEPCI_{old}$, and $CEPCI_{2021}$ are the IEC in the older year, IEC in 2021, CEPCI of the older year, and CEPCI of 2021, respectively. We use a value of 708 for $CEPCI_{2021}$.

$$(S.22) \quad IEC_{old} = f_{installation} \bullet PEC$$

$$(S.23) \quad IEC_{2021} = IEC_{old} \bullet \left(\frac{CEPCI_{2021}}{CEPCI_{old}}\right)$$

Table S.6. Installation factors used in the present study.

Equipment	Installation Factor
Centrifugal fans	1.4
PVC packing	3.2
Pump	4
Crystallizer (pellet reactor)	2.2
Furnace (calciner)	2.5
Fluidized-bed dryer (slaker)	2.2
H_2O/CO_2 electrolyzer	1.2
Catalyst/membrane	1.2
Pressure swing adsorber	2.5

The inside battery limit (ISBL) cost is simply the summation of all 2021 IECs, Eq. S.24. From the ISBL, an estimate of the OSBL, engineering, and contingency costs can be generated. The OSBL was assumed to be 40% of the ISBL, consistent with typical initial estimates of new petrochemical plants.[16] The engineering and contingency costs were assumed to be 10% and 30% of the summation of ISBL and OSBL, respectively.[16] Finally, the fixed capital investment (FCI) or the capital expenditures (CAPEX) is the summation of ISBL, OSBL, engineering, and contingency costs, as shown by Eq. S.25. Adding 15% of the summation of ISBL and OSBL as the working capital (WC) would give the total FCI (TFCI). To annualize the TFCI or the FCI, a multiplication factor called the capital recovery factor (CRF) is used, Eq. S.26 and S.27. In Eq. S.26, i is the interest rate and t is the plant lifetime.

(S.24) $ISBL = \sum IEC_i$

(S.25) $FCI = CAPEX = ISBL + OSBL + Engineering + Contingency$

(S.26) $CRF = \frac{i(1+i)^t}{[(1+i)^t - 1]}$

(S.27) $Annual\ CAPEX = CAPEX \bullet CRF$

In the present work, the interest rate is assumed to be 7% for DACC and RWGS, and 10.1% for PEMWE and CO_2ER. The lifetime is assumed to be 25 years for DACC and RWGS, and 11 years for PEMWE and CO_2ER. The higher interest rates and lower lifetimes for electrolysis systems are

consistent with the 2020 H_2A production model for a future central PEM electrolysis system.[17] Similarly, the lower interest rates and higher lifetimes of DACC and RWGS are consistent with literature assumptions.[1,9] For all processes, the plant utilization rate is assumed to be 90%, meaning that the plants operate 328.5 days at 24 hrs/day in a year.

S.2.2. Operational costs

The considered fixed operational costs ($OPEX_{fixed}$) here consist of operating labor, supervision, direct salary overhead, maintenance, property taxes and insurance, rent of land, general plant overhead, and environmental charges, consistent with the method used by Towler and Sinnot.[16] Table S.7 reports the assumptions made for estimating each component of the $OPEX_{fixed}$. The variable OPEX ($OPEX_{var}$) consists of raw materials, utilities, and any consumable (e.g., catalysts). Table S.8 summarizes the prices used for estimating these cost components. The costs of natural gas and renewable electricity are assumed to be constant at $5.03/GJ and $45/MWh, respectively. It is worth noting, however, that the $45/MWh represents a rough average for solar photovoltaic (PV) electricity. Finally, the total $OPEX_{annual}$ is the sum of $OPEX_{fixed}$ and $OPEX_{var}$, Eq. S.28.

(S.28) $OPEX_{annual} = OPEX_{fixed} + OPEX_{var}$

Table S.7. Assumptions of each operational cost component.

Component	Percentage	of
Supervision	25%	Operating labor
Direct salary overhead	50%	(Operating labor + Supervision)
Maintenance	3%	ISBL
Property taxes & insurance	1%	ISBL
Rent of land	1%	(ISBL + OSBL)
General plant overhead	50%	(labor + maintenance)
Allocated environmental charges	1%	(ISBL + OSBL)

Table S.8. Prices of components used in the techno-economic calculations.

Component	Price	Source/*Notes*
KOH ($/t)	450	Price of caustic potash in the U.S. in December of 2020 based on data from ChemAnalyst[23]
CaCO$_3$ ($/t)	7	*Back calculated from discussion in* Keith et al.[1]
H$_2$O ($/t)	0.1	Keith et al.[1]
HCl ($/t)	84.77	Average 1-yr price in 2017-2018 based on data from Intratec[24]
Electricity ($/MWh)	45	*Rough average considering $30/MWh and $60/MWh are the minimum and maximum possible prices*
Natural gas ($/GJ)	4.52	(2050 price) in the 2023 U.S. EIA annual energy outlook report[25]

S.3. Mass flow rates and fractions of major DACC equipment

Tables S.9 – S.12 summarize the stream total mass flow rates and the component mass fractions of major equipment (i.e., air contactor, pellet reactor, calciner, and slaker) from our 1 Mt-CO$_2$/yr model. Similar calculations were performed for the scaled up versions that were integrated with CO$_2$ electrolysis and RWGS, which are shown in Tables S.13 – S.16 and Tables S.17 – S.20, respectively.

1 Mt-CO$_2$ DACC plant:

Table S.9. Mass flow rate and fraction information of the modeled air contactor units for the 1 Mt-CO$_2$/yr plant.

	Inlet Air	Inlet Solvent	Outlet Air	Outlet Solvent
$\dot{m}_{tot}$ [t/hr]	251,000.0	5,468.9	251,360.8	5,108.1
CO$_2$	0.000600		0.000160	0.000001
H$_2$O	0.009800	0.884299	0.011661	0.844938
K$^+$		0.071632		0.076691
CO$_3^{2-}$		0.029788		
O$_2$	0.230000	0.000001	0.229670	0.000004
N$_2$	0.759600	0.000002	0.758510	0.000007
HCO$_3^-$		0.000004		0.062385
H$_3$O$^+$				
OH$^-$		0.014274		0.015972
KOH				
K$_2$CO$_3$				
KHCO$_3$				
Ca^{2+}				
Ca(OH)$_2$				
CaCO$_3$				
CaO				
CH$_4$				
C$_2$H$_6$				
CaOH$^+$				

Table S.10. Mass flow rate and fraction information of the modeled pellet reactors for the 1 Mt-CO_2/yr plant.

	Cap. Sol.	$CaCO_3$ (cal.)	$CaCO_3$ (rec.)	$CaCO_3$ (mkup)	$Ca(OH)_2$	Liq. Rec.	$CaCO_3$ out	Liq. Out
$\dot{m}_{tot}$ [t/hr]	34,787.9	6.0	4.7	3.6	802.0	170,512.8	277.6	205,377.7
CO_2								
H_2O	0.8842				0.7220	0.8804		0.8877
K^+	0.0715				0.0038	0.0706		0.0706
CO_3^{2-}	0.0303							0.0249
O_2								
N_2								
HCO_3^-					0.0013	0.0254		
H_3O^+								
OH^-	0.0139				0.1260	0.0236		0.0166
KOH								
K_2CO_3	0.8842							
$KHCO_3$	0.0716							
Ca^{2+}	0.0303				0.1469			
$Ca(OH)_2$								
$CaCO_3$		1.0000	1.0000	1.0000			1.000	0.0002
CaO								
CH_4								
C_2H_6	0.01393							
$CaOH^+$								

Table S.11. Mass flow rate and fraction information of the modeled calciners for the 1 Mt-CO_2/yr plant.

	$CaCO_3$ in	$CaCO_3$ fines	CH_4	O_2/N_2	Solids out	Gases out
$\dot{m}_{tot}$ [t/hr]	227.6	22.6	12.8	55.4	170.8	197.5
CO_2						0.832039
H_2O						0.144985
K^+						
CO_3^{2-}						
O_2				0.956000		0.010634
N_2				0.044000		0.012342
HCO_3^-						
H_3O^+						
OH^-						
KOH						
K_2CO_3						
$KHCO_3$						
Ca^{2+}						
$Ca(OH)_2$						
$CaCO_3$	1.000000	1.000000			0.035144	
CaO					0.964856	
CH_4			1.000000			
C_2H_6						
$CaOH^+$						

Table S.12. Mass flow rate and fraction information of the modeled slakers for the 1 Mt-CO_2/yr plant.

	CaO in	H_2O	H_2O wash	Recycled $Ca(OH)_2$
$\dot{m}_{tot}$ [t/hr]	164.8	70.2	567.0	802.0
CO_2			0.000001	
H_2O		0.999994	0.990877	0.722017
K^+			0.005443	0.003848
CO_3^{2-}				
O_2				
N_2				
HCO_3^-			0.001819	0.001287
H_3O^+		0.000003		
OH^-		0.000003	0.001861	0.125975
KOH				
K_2CO_3				
$KHCO_3$				
Ca^{2+}				0.146873
$Ca(OH)_2$				
$CaCO_3$				
CaO	1.000000			
CH_4				
C_2H_6				
$CaOH^+$				

DACC-RWGS plant:

Table S.13. Mass flow rate and fraction information of the modeled air contactor units for the DACC plant that was integrated with RWGS.

	Inlet Air	Inlet Solvent	Outlet Air	Outlet Solvent
$\dot{m}_{tot}$ [t/hr]	525,531.3	16,788.4	526,296.7	16,023.0
CO_2	0.000600		0.000139	0.000001
H_2O	0.009800	0.883743	0.011701	0.854033
K^+		0.072352		0.075808
CO_3^{2-}		0.028687		
O_2	0.230000	0.000001	0.229665	0.000004
N_2	0.759600	0.000002	0.758495	0.000007
HCO_3^-		0.000004		0.051534
H_3O^+				0.000000
OH^-		0.015212		0.018613
KOH				
K_2CO_3				
$KHCO_3$				
Ca^{2+}				
$Ca(OH)_2$				
$CaCO_3$				
CaO				
CH_4				
C_2H_6				
$CaOH^+$				

Table S.14. Mass flow rate and fraction information of the modeled pellet reactors for the DACC plant that was integrated with RWGS.

	Cap. Sol.	$CaCO_3$ (*cal.*)	$CaCO_3$ (rec.)	$CaCO_3$ (mkup)	$Ca(OH)_2$	Liq. Rec.	$CaCO_3$ out	Liq. Out
$\dot{m}_{tot}$ [t/hr]	103,667.5	12.6	9.9	7.4	610.8	469,110.9	581.3	572,837.7
CO_2								
H_2O	0.8837				0.2517	0.8775		0.8851
K^+	0.0722				0.0011	0.0723		0.0723
CO_3^{2-}	0.0291							0.0256
O_2								
N_2								
HCO_3^-					0.0004	0.0260		
H_3O^+						0.0000		
OH^-	0.0149				0.3431	0.0242		0.0169
KOH								
K_2CO_3								
$KHCO_3$								
Ca^{2+}					0.4038			
$Ca(OH)_2$								
$CaCO_3$		1.0000	1.0000	1.0000			1.0000	0.0001
CaO								
CH_4								
C_2H_6								
$CaOH^+$								

Table S.15. Mass flow rate and fraction information of the modeled calciners for the DACC plant that was integrated with RWGS.

	$CaCO_3$ in	$CaCO_3$ fines	CH_4	O_2/N_2	Solids out	Gases out
$\dot{m}_{tot}$ [t/hr]	581.3	47.2	26.7	116.1	357.7	413.6
CO_2						0.8317
H_2O						0.1448
K^+						
CO_3^{2-}						
O_2				0.9560		0.0111
N_2				0.0440		0.0123
HCO_3^-						
H_3O^+						
OH^-						
KOH						
K_2CO_3						
$KHCO_3$						
Ca^{2+}						
$Ca(OH)_2$						
$CaCO_3$	1.0000	1.0000			0.0351	
CaO					0.9649	
CH_4			1.0000			
C_2H_6						
$CaOH^+$						

Table S.16. Mass flow rate and fraction information of the modeled slakers for the DACC plant that was integrated with RWGS.

	CaO in	H_2O	H_2O wash	Recycled $Ca(OH)_2$
$\dot{m}_{tot}$ [t/hr]	345.1	147.0	118.7	610.8
CO_2				
H_2O		1.0000	0.9909	0.2517
K^+			0.0054	0.0011
CO_3^{2-}				
O_2				
N_2				
HCO_3^-			0.0018	0.0004
H_3O^+				
OH^-			0.0019	0.3431
KOH				
K_2CO_3				
$KHCO_3$				
Ca^{2+}				0.4038
$Ca(OH)_2$				
$CaCO_3$				
CaO	1.0000			
CH_4				
C_2H_6				
$CaOH^+$				

DACC-CO₂ER plant:

Table S.17. Mass flow rate and fraction information of the modeled air contactor units for the DACC plant that was integrated with CO_2 electrolysis.

	Inlet Air	Inlet Solvent	Outlet Air	Outlet Solvent
$\dot{m}_{tot}$ [t/hr]	502,784.4	15,780.5	15,001.7	503,563.1
CO_2	0.000600		0.000139	0.000001
H_2O	0.009800	0.884986	0.011792	0.854660
K^+		0.071633		0.075352
CO_3^{2-}		0.028199		
O_2	0.230000	0.000001	0.229644	0.000004
N_2	0.759600	0.000001	0.758425	0.000007
HCO_3^-		0.000004		0.051571
H_3O^+				
OH^-		0.015176		0.018404
KOH				
K_2CO_3				
$KHCO_3$				
Ca^{2+}				
$Ca(OH)_2$				
$CaCO_3$				
CaO				
CH_4				
C_2H_6				
$CaOH^+$				

Table S.18. Mass flow rate and fraction information of the modeled pellet reactors for the DACC plant that was integrated with CO_2 electrolysis.

	Cap. Sol.	$CaCO_3$ (cal.)	$CaCO_3$ (rec.)	$CaCO_3$ (mkup)	$Ca(OH)_2$	Liq. Rec.	$CaCO_3$ out	Liq. Out
$\dot{m}_{tot}$ [t/hr]	97,557.2	12.0	9.5	7.1	1,606.6	446,086.4	556.1	544,722.5
CO_2								
H_2O	0.8849				0.7220	0.8800		0.8874
K^+	0.0716				0.0038	0.0709		0.0709
CO_3^{2-}	0.0287							0.0248
O_2								
N_2								
HCO_3^-					0.0013	0.0253		
H_3O^+					0.0000	0.0000		
OH^-	0.0149				0.1260	0.0238		0.0168
KOH								
K_2CO_3								
$KHCO_3$								
Ca^{2+}					0.1469			
$Ca(OH)_2$								
$CaCO_3$		1.0000	1.0000	1.0000			1.0000	0.0001
CaO								
CH_4								
C_2H_6								
$CaOH^+$								

Table S.19. Mass flow rate and fraction information of the modeled calciners for the DACC plant that was integrated with CO_2 electrolysis.

	$CaCO_3$ in	$CaCO_3$ fines	CH_4	O_2/N_2	Solids out	Gases out
$\dot{m}_{tot}$ [t/hr]	556.1	45.2	25.5	111.3	342.2	396.0
CO_2						0.8314
H_2O						0.1449
K^+						
CO_3^{2-}						
O_2				0.9560		0.0114
N_2				0.0440		0.0124
HCO_3^-						
H_3O^+						
OH^-						
KOH						
K_2CO_3						
$KHCO_3$						
Ca^{2+}						
$Ca(OH)_2$						
$CaCO_3$	1.0000	1.0000			0.0351	
CaO					0.9649	
CH_4			1.0000			
C_2H_6						
$CaOH^+$						

Table S.20. Mass flow rate and fraction information of the modeled slakers for the DACC plant that was integrated with CO_2 electrolysis.

	CaO in	H_2O	H_2O wash	Recycled $Ca(OH)_2$
$\dot{m}_{tot}$ [t/hr]	330.2	140.6	1,135.8	1,606.6
CO_2				
H_2O		1.0000	0.9909	0.7220
K^+			0.0054	0.0038
CO_3^{2-}				
O_2				
N_2				
HCO_3^-			0.0018	0.0013
H_3O^+				0.0000
OH^-			0.0019	0.1260
KOH				
K_2CO_3				
$KHCO_3$				
Ca^{2+}				0.1469
$Ca(OH)_2$				
$CaCO_3$				
CaO	1.0000			
CH_4				
C_2H_6				
$CaOH^+$				

S.4. Technical metrics calculations

S.4.1. Carbon efficiency

Carbon efficiency is defined as the moles of carbon in the desired product over the moles of carbon in the reactants. In the present work, we used Eq. S.29 to calculate this metric.

(S.29) $\quad CE = \dfrac{n_{C,CO}}{n_{C,CO_2/CH_4}}$

S.4.2. Energy consumption

The energy consumption of DACC was calculated using Aspen Energy Analyzer after implementing heat integration. As found in the text, these values were found to be 577.7 and 550.3 MW_{th}. For CO_2 electrolysis, we used Eq. S.30, where V_{cell}, n_{e^-}, F, FE_{CO}, and MW_{CO} are the cell voltage, number of required electrons, Faraday's constant, Faradaic efficiency of CO, and molecular weight of CO, respectively.

(S.30) $\quad E_{CO_2ER} \left(\dfrac{MWh}{t-CO}\right) = \dfrac{V_{cell} \bullet n_{e^-} \bullet F}{FE_{CO} \bullet MW_{CO}} \bullet \dfrac{3600 \bullet 10^6}{10^6}$

For water electrolysis, we use 4.3 $kWh/Nm^3\text{-}H_2$ as the electricity consumption. To get the electricity consumption in MWh/t-CO, we use Eq. S.31, where E°_{PEMWE}, MW_{H2}, and $z_{H2/syngas}$ are the electricity consumption of PEMWE in $kWh/Nm^3\text{-}H_2$, molecular weight of H_2, and mass ratio of H_2 to syngas, respectively.

(S.31) $\quad E_{PEMWE} \left(\dfrac{MWh}{t-CO}\right) = E^o_{PEMWE} \left(\dfrac{8.314 \bullet 273.15}{101325}\right) \bullet (1000) \bullet z_{H_2/syngas}$

For RWGS and SMR, we reference Rezaei and Dzuryk's study results.[9]

S.5. Supplementary figures

S.5.1. Comparison of our and Keith et al.'s modeling results

Fig. S.1. shows the mass flow differences of our and Keith et al.'s modeling results for the major components in the air contactor and calciner. Note the minimal difference of mass flow rate of all components except for O_2, which is explained by the fact that we used lower amounts

of methane in the calciner to achieve a net zero heat duty. The figure highlights the consistency between our and Keith et al.'s[1] results.
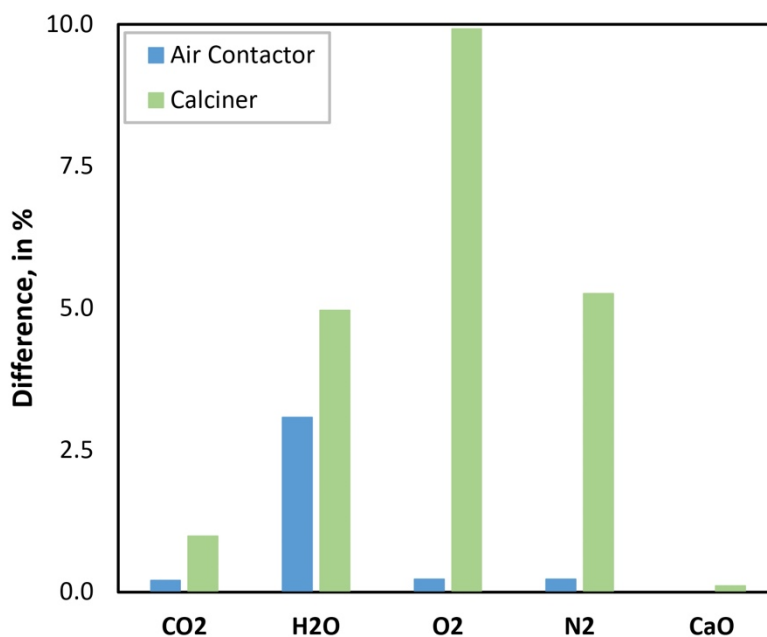

Figure S.1. Mass flow rate difference between our and Keith et al.'s modeling results. Blue bars (left): Air contactor; Green bars (right): Calciner.

S.5.2. Additional future scenarios

Fig. S.2. shows the same data in Fig. 7 of the main text with the addition of a case in which the CO_2 tax and tax credit are \$0/t-CO_2. We discuss the results further in the main text, but in short, the electricity price targets that would allow DACC-PEMWE-CO_2ER to begin competing economically with conventional syngas production methods are ≤\$18/MWh, ≤\$19/MWh, ≤\$21/MWh, ≤\$23/MWh for the 2.50, 2.25, 2.00, and 1.75 V cases, respectively.
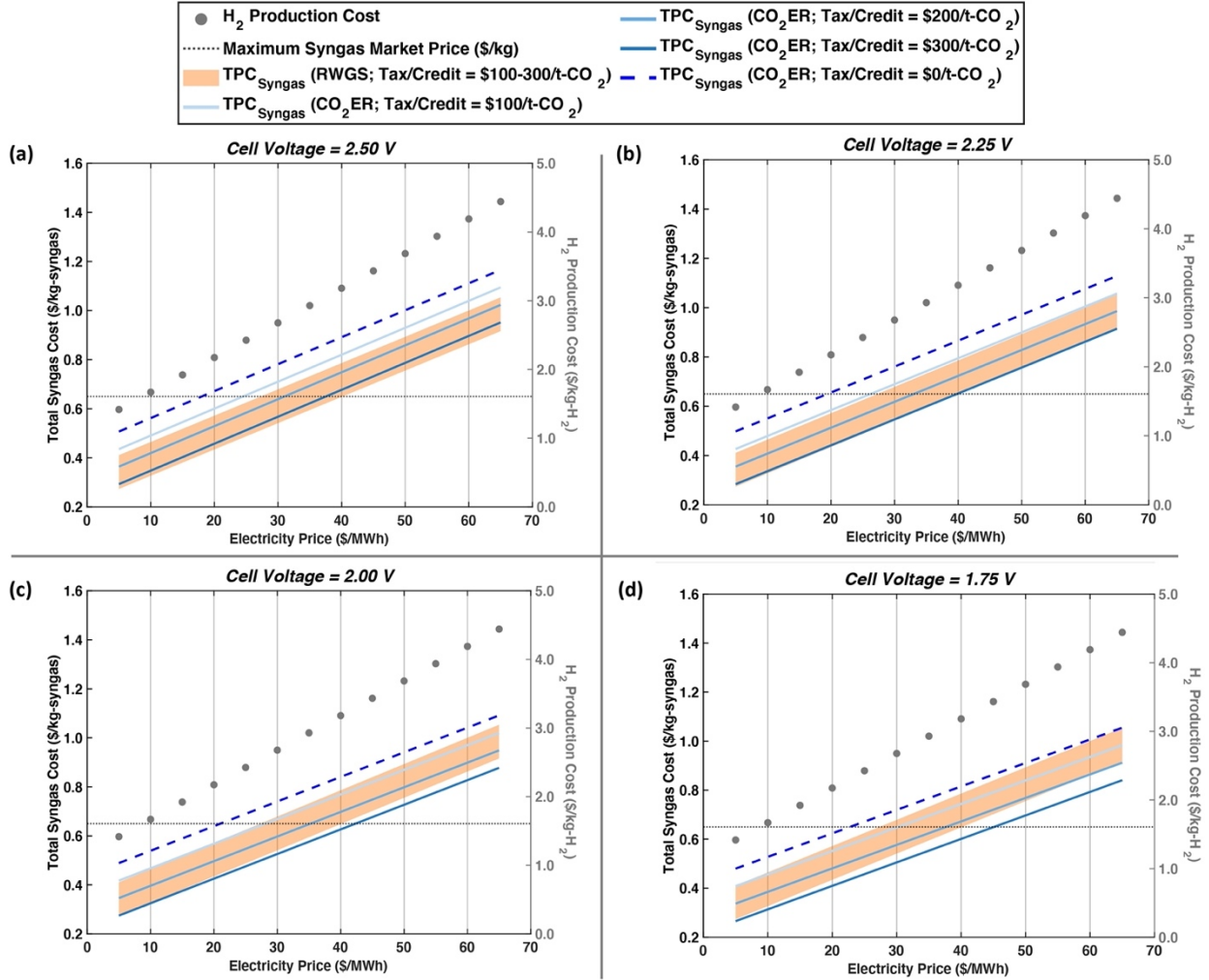
Figure S.2. Future scenarios of DACC-PEMWE-RWGS (shaded orange) and DACC-PEMWE-CO_2ER (blue solid and dashed lines) routes, showing the maximum syngas price via conventional methods (dotted black line) and the H_2 production cost (grey dots). Note the different shades in the blue solid lines represent different CO_2 tax and tax credits. The blue dashed line is showing the additional case of $0/t-$CO_2$ tax and tax credit.

Fig. S.3. shows the same data in Fig. 7 of the main text with the addition of a case in which the CO_2 tax and tax credit are $130/t-$CO_2$. This value is what is given in section 45Q of the U.S. internal revenue code for CO_2 captured by DACC and used to make fuels or chemicals. Similar to Fig. S.2., we provide further discussion of the results in the main text. The main takeaway, however, is that the electricity price targets that would allow DACC-PEMWE-CO_2ER to begin competing economically with conventional syngas production methods are ≤$26/MWh, ≤$28/MWh, ≤$30/MWh, and ≤$32/MWh for the 2.50, 2.25, 2.00, and 1.75 V cases, respectively.
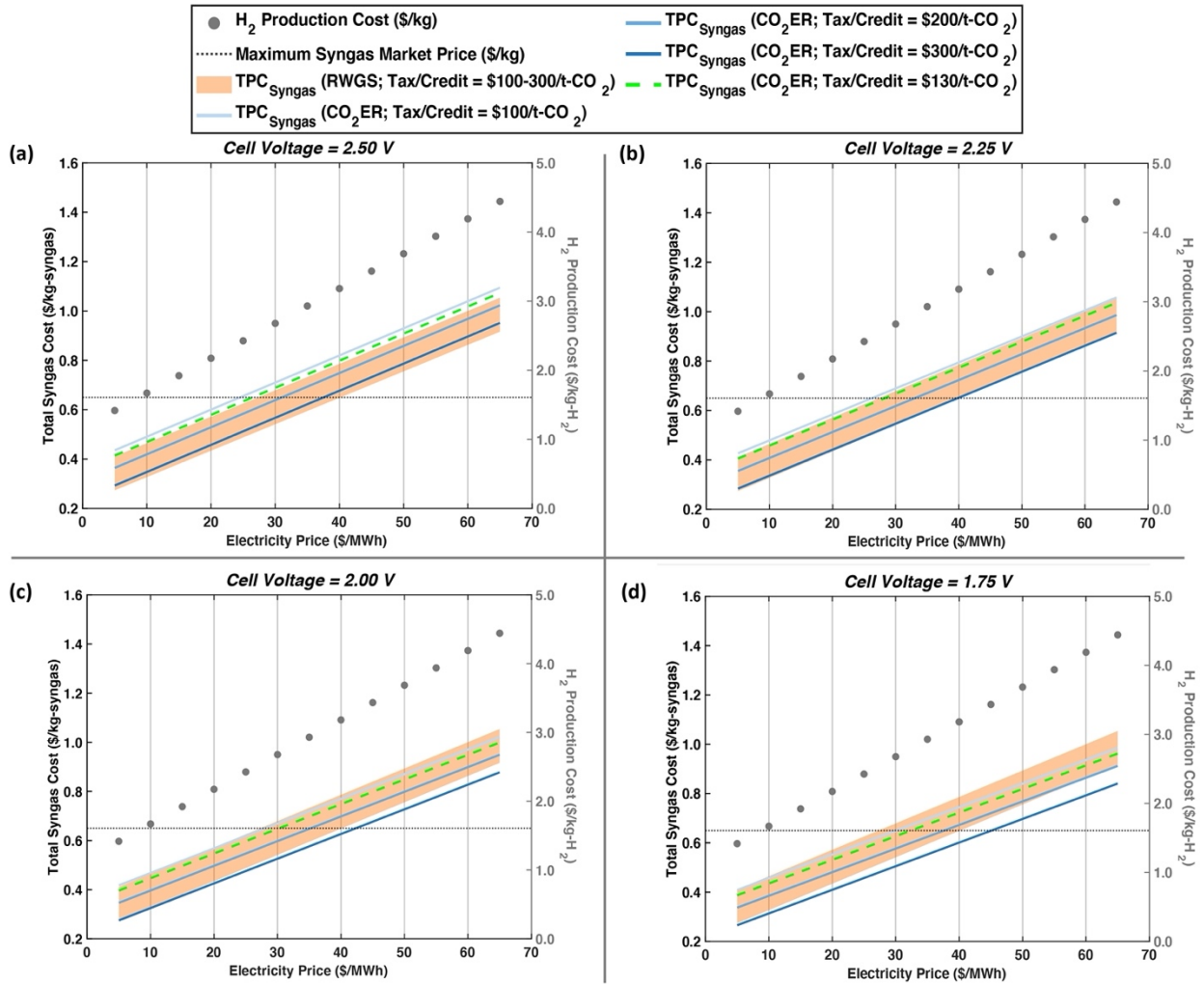
Figure S.3. Future scenarios of DACC-PEMWE-RWGS (shaded orange) and DACC-PEMWE-CO$_2$ER (blue solid lines and dashed green line) routes, showing the maximum syngas price via conventional methods (dotted black line) and the H$_2$ production cost (grey dots). Note the different shades in the blue solid lines represent different CO$_2$ tax and tax credits. The green dashed line is showing the additional case of $130/t-CO$_2$ tax and tax credit.
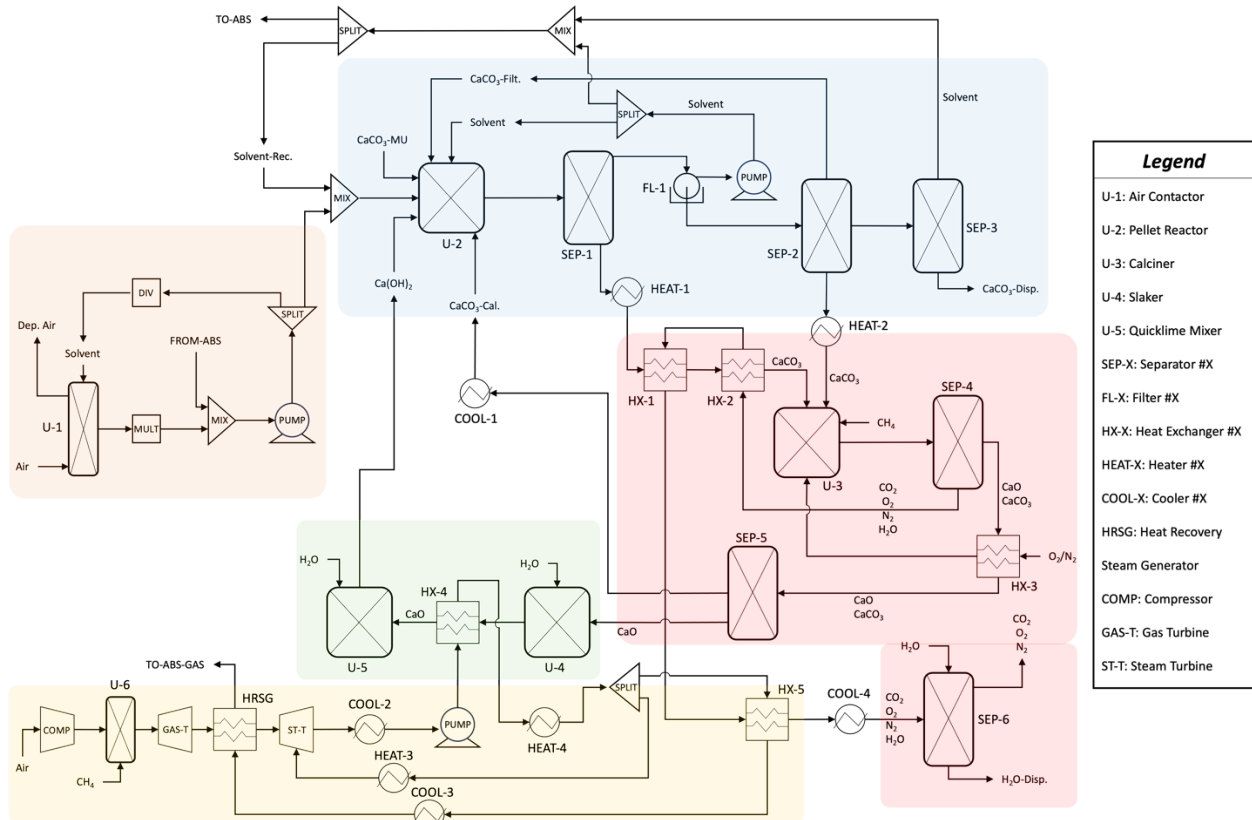
S.5.3. Aspen Plus process flow diagram of the DACC plant

Figure S.4. Process flow diagram of the DACC plant that was built in Aspen Plus. The orange, blue, pink, green, and yellow shaded regions represent the air contactor, pellet reactor, calciner, slaker, and power island sections, respectively. Note that we are assuming the generated CO_2 from the methane combustion is captured using an absorber, but we are not modeling that absorber here.

References

1. Keith DW, Holmes G, St. Angelo D, Heidel K. A process for capturing CO_2 from the stmosphere. Joule. 2018 Aug;2(8):1573–94.
2. Holmes G, Keith DW. An air–liquid contactor for large-scale capture of CO_2 from air. Phil Trans R Soc A. 2012 Sep 13;370(1974):4380–403.
3. Heidel K, Keith D, Singh A, Holmes G. Process design and costing of an air-contactor for air-capture. Energy Procedia. 2011;4:2861–8.
4. Sabatino F, Grimm A, Gallucci F, van Sint Annaland M, Kramer GJ, Gazzani M. A comparative energy and costs assessment and optimization for direct air capture technologies. Joule. 2021 Aug;5(8):2047–76.
5. Marchese M, Buffo G, Santarelli M, Lanzini A. CO_2 from direct air capture as carbon feedstock for Fischer-Tropsch chemicals and fuels: Energy and economic analysis. Journal of CO_2 Utilization. 2021 Apr 1;46:101487.
6. Chen CC, Britt HI, Boston JF, Evans LB. Local composition model for excess Gibbs energy of electrolyte systems. Part I: Single solvent, single completely dissociated electrolyte systems. AIChE Journal. 1982;28(4):588–96.
7. Pinsent BRW, Pearson L, Roughton FJW. The kinetics of combination of carbon dioxide with hydroxide ions. Trans Faraday Soc. 1956 Jan 1;52(0):1512–20.
8. Edwards TJ, Maurer G, Newman J, Prausnitz JM. Vapor-liquid equilibria in multicomponent aqueous solutions of volatile weak electrolytes. AIChE Journal. 1978;24(6):966–76.
9. Rezaei E, Dzuryk S. Techno-economic comparison of reverse water gas shift reaction to steam and dry methane reforming reactions for syngas production. Chemical Engineering Research and Design. 2019 Apr 1;144:354–69.
10. Juneau M, Vonglis M, Hartvigsen J, Frost L, Bayerl D, Dixit M, et al. Assessing the viability of K-Mo_2C for reverse water–gas shift scale-up: molecular to laboratory to pilot scale. Energy Environ Sci. 2020 Aug 13;13(8):2524–39.
11. Adelung S, Maier S, Dietrich RU. Impact of the reverse water-gas shift operating conditions on the power-to-liquid process efficiency. Sustainable Energy Technologies and Assessments. 2021 Feb 1;43:100897.
12. König DH, Baucks N, Dietrich RU, Wörner A. Simulation and evaluation of a process concept for the generation of synthetic fuel from CO_2 and H_2. Energy. 2015 Nov 1;91:833–41.
13. Wen G, Ren B, Wang X, Luo D, Dou H, Zheng Y, et al. Continuous CO_2 electrolysis using a CO_2 exsolution-induced flow cell. Nat Energy. 2022 Oct;7(10):978–88.
14. Sone Y, Ekdunge P, Simonsson D. Proton conductivity of Nafion 117 as measured by a four-electrode AC ompedance method. J Electrochem Soc. 1996 Apr 1;143(4):1254.

15. Wen G. Nanostructured materials and electrodes engineering for efficient CO_2 conversion [Internet]. [Waterloo, Ontario, Canada]: University of Waterloo; 2020 [cited 2023 May 19]. Available from: http://hdl.handle.net/10012/16283

16. Towler G, Sinnott R. Capital Cost Estimating. In: Chemical Engineering Design [Internet]. Elsevier; 2013 [cited 2023 Feb 20]. p. 307–54. Available from: https://linkinghub.elsevier.com/retrieve/pii/B9780080966595000079

17. NREL. H_2A: Hydrogen Analysis Production Models [Internet]. 2020 [cited 2023 Feb 20]. Available from: https://www.nrel.gov/hydrogen/h2a-production-models.html

18. Sodiq A, Abdullatif Y, Aissa B, Ostovar A, Nassar N, El-Naas M, et al. A review on progress made in direct air capture of CO_2. Environmental Technology & Innovation. 2023 Feb 1;29:102991.

19. Erans M, Sanz-Pérez ES, Hanak DP, Clulow Z, Reiner DM, Mutch GA. Direct air capture: process technology, techno-economic and socio-political challenges. Energy Environ Sci. 2022;10.1039.D1EE03523A.

20. Moreno-Gonzalez M, Berger A, Borsboom-Hanson T, Mérida W. Carbon-neutral fuels and chemicals: Economic analysis of renewable syngas pathways via CO_2 electrolysis. Energy Conversion and Management. 2021 Sep 15;244:114452.

21. Badgett A, Ruth M, Crow A, Grim G, Chen Y, Hu L, et al. An economic analysis of the role of materials, system engineering, and performance in electrochemical carbon dioxide conversion to formate. Journal of Cleaner Production. 2022 Jun 1;351:131564.

22. Kannangara M, Shadbahr J, Vasudev M, Yang J, Zhang L, Bensebaa F, et al. A standardized methodology for economic and carbon footprint assessment of CO_2 to transport fuels: Comparison of novel bicarbonate electrolysis with competing pathways. Applied Energy. 2022 Nov 1;325:119897.

23. ChemAnalyst. Caustic Potash Price Trend and Forecast [Internet]. 2023 [cited 2023 Jul 14]. Available from: https://www.chemanalyst.com/Pricing-data/caustic-potash-1212

24. INTRATEC. INTRATEC. 2018 [cited 2023 Jul 24]. Hydrochloric Acid Price. Available from: https://www.intratec.us/chemical-markets/hydrochloric-acid-price

25. U.S. Energy Information Administration. Annual Energy Outlook 2023 – Table 13 [Internet]. 2023 [cited 2023 Jul 13]. Available from: https://www.eia.gov/outlooks/aeo/data/browser/#/?id=13-AEO2023&cases=ref2023&sourcekey=0.